Int. J. Electrochem. Sci., 13 **(2018)** 23 – 28, doi: 10.20964/2018.01.41

International Journal of
ELECTROCHEMICAL
SCIENCE
www.electrochemsci.org

Short Communication

Hierarchical MoO_2/rGO Composite as a High-Performance Anode Material for Lithium-Ion Batteries

Shi Li [1], *Zhigao Luo* [1,*], *Xinxin Cao* [1], *Guozhao Fang* [1], *Shuquan Liang* [1, 2,*]

[1] School of Materials Science and Engineering, Central South University, Changsha 410083, Hunan, China
[2] Key Laboratory of Nonferrous Metal Materials Science and Engineering, Ministry of Education, Central South University, Changsha 410083, Hunan, China
[*]E-mail: zhigao820@csu.edu.cn, lsq@csu.edu.cn

Received: 1 September 2017 / *Accepted:* 31 October 2017 / *Online Published:* 1 December 2017

The rational design of composites containing transition metal oxides and graphene has received great attention because of the excellent electrochemical performance and potential applications of these materials in the energy storage field. The introduction of graphene promotes the electronic conductivity and lithium or sodium storage capacity of the hybrid electrode. We report the synthesis of a hierarchical MoO_2/rGO composite. As a proof-of-concept application, the as-synthesized MoO_2/rGO exhibits good electrochemical performance including a high specific capacity and a high rate stability.

Keywords: MoO_2; Graphene; Lithium-ion battery; Anode material

1. INTRODUCTION

MoO_2 is a special kind of transition metal oxide (TMO) with a distorted rutile-type structure [1, 2]. Compared to other types of TMOs, MoO_2 has been recognized for its low electrical resistivity, high density, and good chemical and thermal stabilities [3]. When applied as a host anode material for lithium-ion batteries, however, only one Li^+ ion can be inserted into the grid structure per formula unit of bulk MoO_2 presenting a low theoretical capacity of 209 mA h g^{-1}, which can be explained by the embedded mechanism. Additionally, the phase change of Li_xMoO_2 from monoclinic ($0 < x < 0.5$) to orthorhombic ($0.45 < x < 0.79$) [4, 5] during the discharge cycle leads to a poor discharge/charge cycle stability. By reducing the MoO_2 particle size to the nanoscale or by improving the electrochemical reaction temperature, the reaction mechanism becomes a conversion mechanism [6, 7]. Theoretically,

four lithium ions can intercalate into the MoO_2 structure, leading to a four-electron redox storage capacity of approximately 838 mA h g^{-1}.

Currently, the main research efforts focus on improving the practical capacity of MoO_2 and optimizing its cycling performance as well as its rate capacity [8, 9]. Different nanostructures were employed to enhance the lithium storage performance of MoO_2 [10, 11]. For most kinds of TMOs, the inevitable volume variation during lithium insertion/extraction leads to material shedding and a loss of electrical connectivity. One way to eliminate the influence is by compositing TMOs with carbon materials [12, 13]. Herein, a hierarchical MoO_2/rGO composite was synthesized by a facile solvothermal approach with DMF as the solvent, which was also employed as the reducing agent. In contrast to previous reports, the as-synthesized MoO_2 shows a nanoparticle morphology rather than nanosheets. The aggregated MoO_2 nanoparticles were dispersed into the interlayer of the corrugated rGO nanosheets. Electrochemical measurements demonstrate that the as-synthesized MoO_2/rGO exhibited good electrochemical performance including a high specific capacity and high rate stability.

2. EXPERIMENTAL

2.1 Materials synthesis

GO was synthesized using the modified Hummer's method [14]. The MoO_2/rGO composite was prepared by a facile solvothermal approach. $(NH_4)_6Mo_7O_{24}\cdot 4H_2O$ (0.5 g) and 5 mL of GO solution (2.5 mg mL^{-1}) were mixed in 30 mL of DMF and dispersed uniformly by ultrasonication, followed by solvothermal synthesis at 200 ℃ for 12 h. Finally, the precipitate was collected by centrifugation, washed with deionized water and anhydrous ethanol several times, and annealed at 600 ℃ for 4 h under an argon atmosphere to obtain the final product. The preparation procedure for bulk MoO_2 is the same as that of the MoO_2/rGO nanocomposites, without adding the GO solution during the solvothermal process.

2.2 Characterization

Power XRD patterns were collected using Rigaku D/max2500 XRD equipment with Cu Kα radiation (λ = 1.54178 Å.). The morphologies of the as-obtained products were analysed by scanning electron microscopy (SEM, FEI Sirion-200). Raman spectra were measured using a Renishaw Invia spectrometer with a laser excitation wavelength of 514.5 nm at room temperature.

2.3 Electrochemical measurements

The electrochemical performance measurements were carried out in a 2016-type coin cell battery. A metallic lithium foil served as the anode. The cathode was fabricated by blending MoO_2/rGO (80% mass fraction) with acetylene black (10% mass fraction) and PVDF (10% mass fraction). The coin cells were assembled in a glove box (Mbraun, Germany) filled with ultra-high-

purity argon using a polypropylene membrane as the separator and a 1 M solution of $LiPF_6$ in ethylene carbonate/dimethyl carbonate (EC/DMC) (1:1 EC:DMC v/v) as the electrolyte. The galvanostatic charge/discharge performances of the electrodes were evaluated at room temperature using a Land battery tester (Land CT 2001A, Wuhan, China). The loading of the MoO_2/rGO anode material for the coin cell test was approximately 1–1.5 mg. Cyclic voltammetry (CV) was measured with an electrochemical workstation (CHI660C, China). Electrochemical impedance spectrometry (EIS) was performed on a ZAHNER-IM6 ex electrochemical workstation (ZAHNER Co., Germany)

3. RESULTS AND DISCUSSION

The XRD pattern of the as-prepared MoO_2/rGO composite is shown in Figure 1a; all diffraction peaks can be indexed to monoclinic MoO_2 with space group P21/c (NO. 14) (JCPDS NO. 73-1249; a = 0.5611 nm, b = 0.4856 nm, c = 0.5628 nm; β = 120.95°) [7, 8]. No impurities were found. The diffraction peaks of rGO in the composite are masked by the partial overlap of the diffraction peaks of MoO_2 at approximately 26°. Raman spectroscopy was applied to identify the structure of rGO, as shown in Fig. 1b. The Raman spectrum of GO displays two Raman bands at 1365.68 cm^{-1} and 1594.06 cm^{-1}, which belong to the well-known D and G bands [14]. The lower intensity of the D band compared to the G band suggests a low defect content in GO. In the MoO_2/rGO composite, the D band exhibits a redshift compared to GO located at 1353.26 cm^{-1}, indicating that GO is reduced to rGO upon formation of the composite [15].

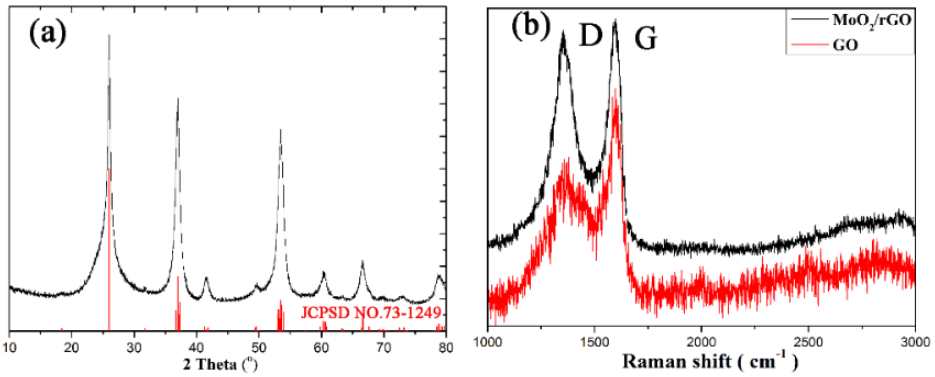

Figure 1. XRD (a) of the as-synthesized MoO_2/rGO composite, Raman spectra (b) of MoO_2/rGO composite (blank) and GO (red). D and G (b) represent the Raman D band and G band of rGO.

The general morphology of the MoO_2/rGO composite is shown in Fig. 2. At low magnification in Figure 2a, the aggregated MoO_2 nanoparticles were dispersed into the interlayer of the corrugated rGO nanosheets. This structure can effectively prevent the aggregation of MoO_2 nanoparticles and accelerate the transportation of electrons during the electrochemical reactions. As shown in Figure 2b, the wavy crumpled nature of the rGO nanosheets was retained in the composite, and the MoO_2 nanoparticles were uniformly entrenched in the rGO nanosheets forming a layer-by-layer structure. In

this structure, the MoO_2 nanoparticles are coated in the interlayer of two rGO nanosheets, facilitating electron transport in the composite and thus promoting the rate cycling performance.

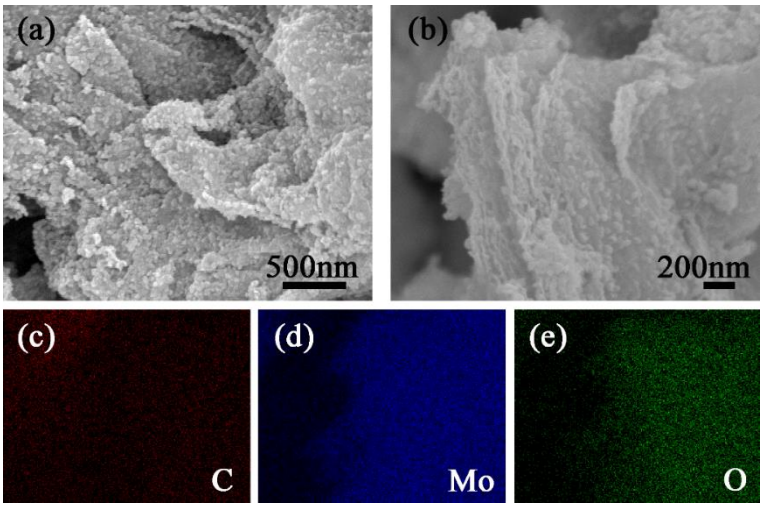

Figure 2. SEM (a, b) and elemental mapping images (c, d, and e) of the as-synthesized MoO_2/rGO composite.

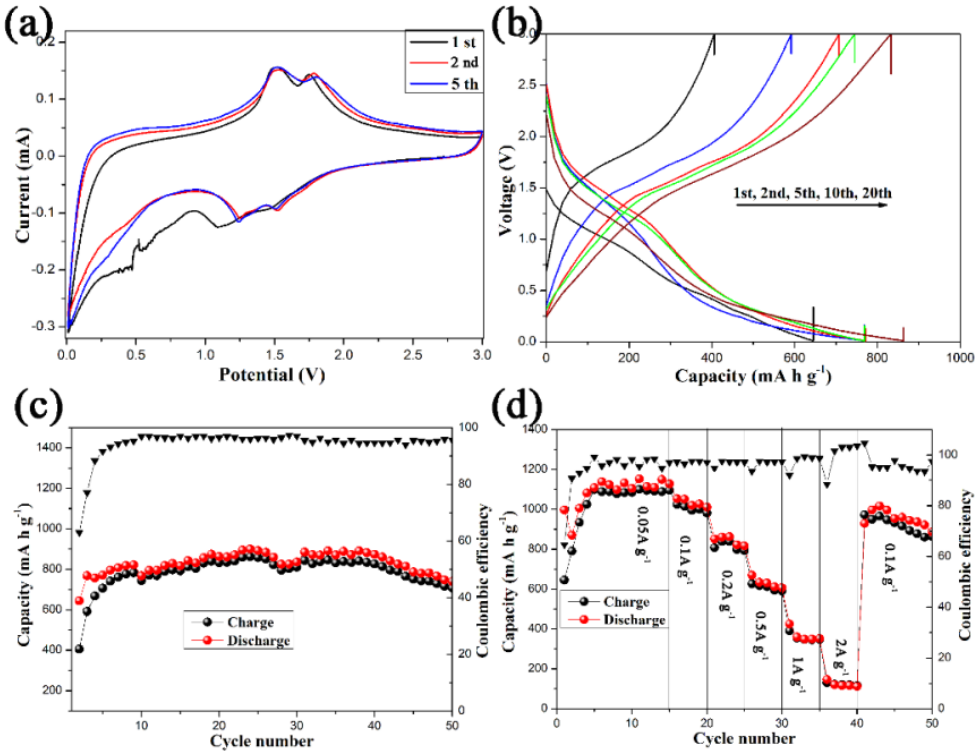

Figure 3. Electrochemical performance of the as-synthesized MoO_2/rGO composite. Cyclic voltammetry (CV) curves (a); galvanostatic charge-discharge curves of the 1st, 2nd, 5th, and 10th cycle (b) at a current density of 100 mA g^{-1}; cycling performance and coulombic efficiency (c) at the current density of 0.1 A g^{-1}; rate performance (d) of the as-synthesized MoO_2/rGO composite.

Fig. 3 shows the electrochemical performance of the MoO_2/rGO composite anode. The CV curves for the 1st, 2nd, and 5th cycles with a scan rate of 0.1 mV s^{-1} are shown in Fig. 3a. In the 1st cycle, the irreversible reduction peak below 1 V disappears in the following cycles corresponding to the formation of an SEI film and the irreversible reduction of the electrolyte. The two highly reversible couples represented by the redox peaks at 1.24/1.52 V and 1.52/1.79 V correspond to the reversible phase transitions of lithium insertion and extraction in Li_xMoO_2[2-4]. The charge/discharge curves of the five selected cycles of the MoO_2/rGO anode at 100 mA g^{-1} are shown in Fig. 3b. The initial discharge and charge capacities are approximately 645 and 406 mA h g^{-1}, respectively, with a relatively low coulombic efficiency of 62.9%. Notably, the capacity rises slowly in subsequent cycles, suggesting a change in the lithiation mechanism of MoO_2. As mentioned before, nanosized MoO_2 exhibits a conversion mechanism [7]. Fig. 3c shows the cycling performance of the MoO_2/rGO at 100 mA g^{-1}. It displays a reversible discharge capacity of 738 mA h g^{-1} after 50 cycles. Fig. 3d shows the rate performance of the MoO_2/rGO evaluated at various current densities from 0.05 to 2 A g^{-1}. Discharge capacities of 1127, 1050, 860, 670, 425, and 151 mA h g^{-1} were observed at 0.05, 0.1, 0.2, 0. 5, 1, and 2 mA g^{-1}, respectively. After charging/discharging at the current density of 2 A g^{-1}, the electrode could recover a high specific capacity of 933 mA h g^{-1} at 100 mA g^{-1}, indicating the excellent high-rate cycling performance of the hierarchical MoO_2/rGO composite.

4. CONCLUSION

A hierarchical MoO_2/rGO composite was prepared by a facile solvothermal approach. MoO_2 nanoparticles were coated in the interlayer of two rGO nanosheets, which facilitated electron transport in the composite. The composite exhibited good electrochemical performance as a LIB anode, including a high specific capacity and a high rate capability up to 2000 mA g^{-1}. The results demonstrate that the MoO_2/rGO composite is a promising material for LIB anodes.

ACKNOWLEDGEMENTS
This work was supported by the National High Technology Research and Development Program of China (863 Program) (Grant no. 2013AA110106), the National Natural Science Foundation of China (Grant no. 51374255, 51302323 and 51572299), the Scientific and Technical Committee Project of Hunan Province (Grant no. 2013GK3100), and the Program for New Century Excellent Talents in University (Grant no. NCET-13-0594).

References

1. Y. Shi, B. Guo, S.A. Corr, Q. Shi, Y.S. Hu, K.R. Heier, L. Chen, R. Seshadri, G.D. Stucky, *Nano lett.*, 9 (2009) 4215-4220.
2. H.J. Zhang, K.X. Wang, X.Y. Wu, Y.M. Jiang, Y.B. Zhai, C. Wang, X. Wei, J.S. Chen, *Adv. Funct. Mater.*, 24 (2014) 3399-3404.
3. J.H. Ku, Y.S. Jung, K.T. Lee, C.H. Kim, S.M. Oh, *J. Electrochem. Soc.*, 156 (2009) A688-A693.
4. L. Zhou, H.B. Wu, Z. Wang, X.W. Lou, *ACS Appl. Mater. Interfaces*, 3 (2011) 4853-4857.
5. X. Zhang, X. Zeng, M. Yang, Y. Qi, *Eur. J. Inorg. Chem.*, 2014 (2014) 352-356.

6. F. Xia, X. Hu, Y. Sun, W. Luo, Y. Huang, *Nanoscale,* 4 (2012) 4707-4711.
7. H.J. Zhang, J. Shu, K.X. Wang, X.T. Chen, Y.M. Jiang, X. Wei, J.S. Chen, *J. Mater. Chem.* A, 2 (2014) 80-86.
8. Y. Sun, X. Hu, W. Luo, Y. Huang, *ACS Nano,* 5 (2011) 7100-7107.
9. X. Liu, H. Xu, Y. Huang, X. Hu, *Phys. Chem.Chem. Phys.*, 18 (2016) 19832-19837.
10. Y. Lei, J. Hu, H. Liu, J. Li, *Mater. Lett.*, 68 (2012) 82-85.
11. W.K. Zhai, Y.M. Xu, X.L. Cheng, S. Gao, X.F. Zhang, H. Zhao, L.H. Huo, *Mater. Lett.*, 145 (2015) 287-290.
12. Q. Yang, Q. Liang, J. Liu, S.Q. Liang, S.S. Tang, P.J. Lu, Y.K. Lu, *Mater. Lett.*, 127 (2014) 32-35.
13. W. Tang, C.X. Peng, C.T. Nai, J. Su, Y.P. Liu, M.V.V. Reddy, M. Lin, K.P. Loh, *Small,* 11 (2015) 2446-2453.
14. Z.G. Luo, J. Zhou, L.R. Wang, G.Z. Fang, A.Q. Pan, S.Q. Liang, *J. Mater. Chem.* A, 4 (2016) 15302-15308.
15. Q. Tang, Z. Shan, L. Wang, X. Qin, *Electrochimica Acta,* 79 (2012) 148-153.